




Functional Analysis and Antivirulence Properties of a New Depolymerase from a Myovirus That Infects *Acinetobacter baumannii* Capsule K45

Hugo Oliveira,^a  Ana Rita Costa,^a Alice Ferreira,^a Nico Konstantinides,^a  Silvio B. Santos,^a Maarten Boon,^b  Jean-Paul Noben,^c  Rob Lavigne,^b Joana Azeredo^a

^aCEB—Centre of Biological Engineering, University of Minho, Braga, Portugal

^bLaboratory of Gene Technology, KU Leuven, Leuven, Belgium

^cBiomedical Research Institute and Transnational University Limburg, Hasselt University, Diepenbeek, Belgium

ABSTRACT *Acinetobacter baumannii* is an important pathogen causative of health care-associated infections and is able to rapidly develop resistance to all known antibiotics, including colistin. As an alternative therapeutic agent, we have isolated a novel myovirus (vB_AbaM_B9) which specifically infects and makes lysis from without in strains of the K45 and K30 capsule types, respectively. Phage B9 has a genome of 93,641 bp and encodes 167 predicted proteins, of which 29 were identified by mass spectrometry. This phage holds a capsule depolymerase (B9gp69) able to digest extracted exopolysaccharides of both K30 and K45 strains and remains active in a wide range of pH values (5 to 9), ionic strengths (0 to 500 mM), and temperatures (20 to 80°C). B9gp69 was demonstrated to be nontoxic in a cell line model of the human lung and to make the K45 strain fully susceptible to serum killing *in vitro*. Contrary to the case with phage, no resistance development was observed by bacteria targeted with the B9gp69. Therefore, capsular depolymerases may represent attractive antimicrobial agents against *A. baumannii* infections.

IMPORTANCE Currently, phage therapy has revived interest for controlling hard-to-treat bacterial infections. *Acinetobacter baumannii* is an emerging Gram-negative pathogen able to cause a variety of nosocomial infections. Additionally, this species is becoming more resistant to several classes of antibiotics. Here we describe the isolation of a novel lytic myophage B9 and its recombinant depolymerase. While the phage can be a promising alternative antibacterial agent, its success in the market will ultimately depend on new regulatory frameworks and general public acceptance. We therefore characterized the phage-encoded depolymerase, which is a natural enzyme that can be more easily managed and used. To our knowledge, the therapeutic potential of phage depolymerase against *A. baumannii* is still unknown. We show for the first time that the K45 capsule type is an important virulence factor of *A. baumannii* and that capsule removal via the recombinant depolymerase activity helps the host immune system to combat the bacterial infection.

KEYWORDS *Acinetobacter baumannii*, antivirulence, bacteriophage, depolymerase

A *Acinetobacter baumannii* is one of the leading nosocomial pathogens, responsible for 2 to 10% of all Gram-negative bacterial hospital infections worldwide (1). It is associated with several hospital-acquired infections (e.g., ventilator-associated pneumonia and bloodstream, urinary tract, and surgical wound infections) and cases of community-acquired infections, mostly in immunocompromised individuals. Mortality rates range from 19 to 54% (1). The treatment of this bacterium is becoming increasingly problematic due to the emergence of multidrug-resistant strains. Many clinical

Citation Oliveira H, Costa AR, Ferreira A, Konstantinides N, Santos SB, Boon M, Noben J-P, Lavigne R, Azeredo J. 2019. Functional analysis and antivirulence properties of a new depolymerase from a myovirus that infects *Acinetobacter baumannii* capsule K45. *J Virol* 93:e01163-18. <https://doi.org/10.1128/JVI.01163-18>.

Editor Julie K. Pfeiffer, University of Texas Southwestern Medical Center

Copyright © 2019 American Society for Microbiology. All Rights Reserved.

Address correspondence to Joana Azeredo, jazeredo@deb.uminho.pt.

H.O. and A.R.C. contributed equally to this article.

Received 5 July 2018

Accepted 8 November 2018

Accepted manuscript posted online 21 November 2018

Published 5 February 2019

isolates are already nonsusceptible to last-resort carbapenem and colistin antibiotics. In fact, carbapenem-resistant *A. baumannii* has been recently listed by the World Health Organization (WHO) as the number one priority pathogen for the development of new antimicrobials (2, 3).

Several virulence factors have been identified in Gram-negative bacilli, among which the capsular structures (k-type) are suggested to be involved in the evasion of microbial defenses and macromolecular antibiotics (4–8). In *A. baumannii*, the existence of at least 106 capsular types may reflect the sophisticated and diverse protective mechanisms developed by this pathogen (9–11).

Bacteriophages and derived enzymes can be seen as an appealing alternative treatment against drug-resistant infections (12). In particular, depolymerases are encoded by some phages to degrade the polysaccharides present in the bacterial capsules, thereby allowing phages to reach the host receptor on the cell surface and initiate infection (13, 14). An extensive *in silico* review of phage depolymerases revealed that most of these enzymes are encoded in phage structural proteins such as tail fibers, baseplates, and necks and that depolymerases can be divided into two main classes: hydrolases and lyases (13). Most phages encode only one or two depolymerase motifs in the same gene, but some can be found encoding multiple depolymerases (15). The presence of depolymerization activity in phages is usually identified by the formation of a halo surrounding phage plaques. Previously, several *A. baumannii* phages encoding depolymerases that infect specific host capsular types (K-types), K1, K2, K3, K9, K19, K27, and K44, have been reported (16–20). However, there is only one study that characterized a recombinant depolymerase demonstrating its ability to degrade capsular polysaccharides extracted from planktonic cells or biofilm matrices (21). Moreover, the therapeutic potential of phage depolymerases is far less explored than that of endolysins and still remains poorly studied in *A. baumannii*.

Our group has been studying the interaction of phage-borne depolymerases with different *Acinetobacter* species (18). In this study, we have isolated and characterized a phage depolymerase targeting *A. baumannii* NIPH 201 which is assigned to the K45 capsule type (22). We have functionally analyzed the primary and secondary structure of the enzyme and determined the conditions under which it is able to degrade the host capsule. The enzyme was demonstrated to have an antivirulence effect against K45 strains in a human alveolar epithelial model, to enhance serum-mediated killing, and to be refractory to the development of resistance under selective pressure.

RESULTS

Novel phage B9 infects K45-type *A. baumannii*. Our initial efforts focused on isolating a lytic phage infecting a K45 strain using the isolation enrichment procedure in which NIPH 201 (a K45 strain) was incubated with raw wastewater treatment samples. Phage B9 was isolated and tested against a panel of *A. baumannii* reference strains of 22 distinct capsular types (Table 1). As expected, phage B9 infected the K45 strain but made lysis from without in a K30 strain. This means that phage B9 does not infect K30. Instead, the phage is capable of lysing K30 by destruction of the cell wall from the outside due to adsorption of multiple phages to a single cell. In agreement, the one-step-growth curve of phage B9 shows it can only replicate inside the K45 strain, with a latent period of 35 min and burst size of 181 phages per infected cell (Fig. 1). Morphologically, phage B9 plaques are characterized by clear and uniform plaques on the host strain with small halos (2 mm in diameter) on 0.6% agar plates (Fig. 2A). Transmission electron microscopy (TEM) images show that B9 features a morphology typical of the *Myoviridae* family, with a 70-nm-diameter icosahedral head and a 110-by-15-nm contractile tail (Fig. 2B).

We further characterized phage B9 using high-throughput sequencing. Phage B9 has a 93,641-bp double-stranded DNA, a GC content of 33.6%, and overall genetic organization composed of 167 predicted open reading frames (ORFs) (Fig. 2C). BLASTN analysis showed an overall genome identity lower than 1% to other phages in the

TABLE 1 Activity spectrum on *A. baumannii* capsular types^a

Strain	K type	B9 phage infectivity	EOP	B9gp46 depolymerase
NIPH 501 ^T	3	—	—	—
NIPH 60	43	—	—	—
NIPH 67	33	—	—	—
NIPH 70	44	—	—	—
NIPH 80	9	—	—	—
NIPH 146	37	—	—	—
NIPH 190	30	—	LFW	+
NIPH 201	45	+	High	+
NIPH 329	46	—	—	—
NIPH 335	49	—	—	—
NIPH 528	9	—	—	—
NIPH 601	47	—	—	—
NIPH 615	48	—	—	—
NIPH 1734	49	—	—	—
NIPH 2390	NA	—	—	—
NIPH 2778	NA	—	—	—
NIPH 2783	NA	—	—	—
NIPH 290	1	—	—	—
NIPH 2061	2	—	—	—
ANC 4097	40	—	—	—
NIPH 4373	NA	—	—	—
J9	11	—	—	—
LUH5554	15	—	—	—
A85	15	—	—	—
RBH2	19	—	—	—
LUH5535	35	—	—	—
BAL_212	57	—	—	—
SGH0703	73	—	—	—

^aDrop test. Phage and recombinant depolymerase were spotted in bacterial lawns to visualize activity. For the phage, the relative efficiency of plating (EOP) was calculated as the titer of the phage (PFU/ml) for each isolate divided by the titer for the propagating host and recorded as high (≥ 0.5) or low (< 0.5). EOP was also performed to distinguish productive infection (lysis) from lysis from without (LFW) by the appearance of cell lysis only in the first dilution(s) for the latter case. K-type, determined capsule structure; NA, capsule structure is not available.

nonredundant database. BLASTP search predicted the function of 77 of the phage B9-encoded proteins, most of which resembled proteins of *Acinetobacter* unclassified myoviruses (Table S1). Based on OrthoVenn analysis, we found that phage B9 shares a maximum of 30 genes with phage YMC13/03/R2096 (98,170 bp, 162 ORFs; GenBank

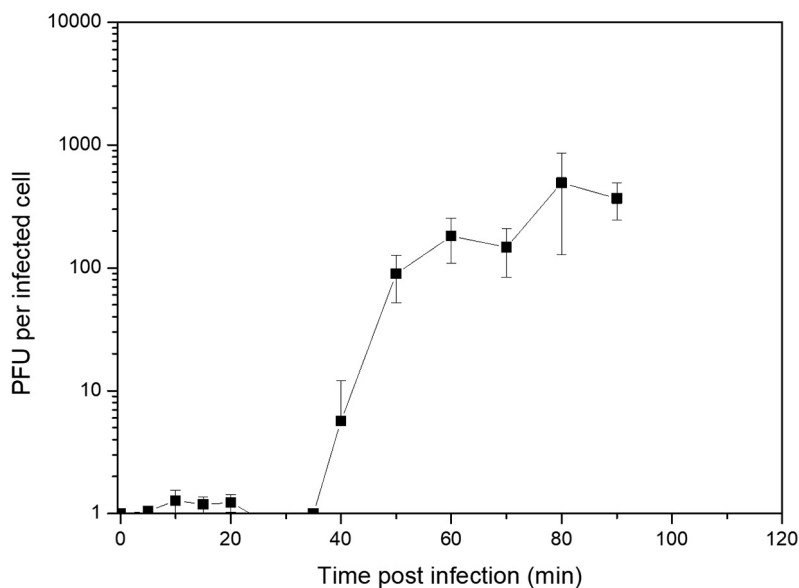


FIG 1 *Acinetobacter baumannii* phage B9 one-step growth curve. The curve was performed using K45 host NIPH 201.

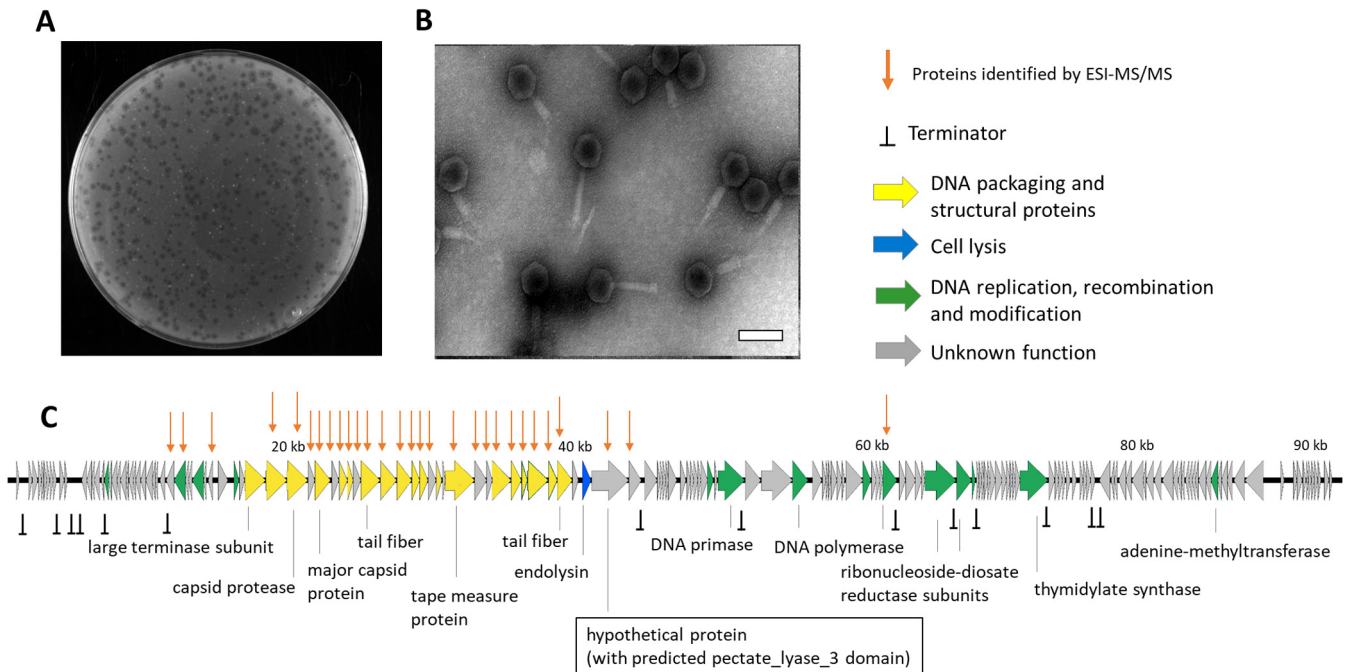


FIG 2 Morphological and genomic analysis of phage B9. (A) Plaques of phage B9 on K45 *A. baumannii* strain NIPH 201. (B) TEM micrographs of phage B9 negatively stained with 2% uranyl acetate. Scale bar indicates 100 nm. (C) Genome map of phage B9 with 167 predicted proteins colored according to their predicted function. Proteins identified by liquid chromatography-electrospray ionization-tandem mass spectrometry (nanoESI-MS/MS) are indicated. The hypothetical protein with the predicted depolymerase domain (pectate_lyase_3) used in this study is also highlighted.

accession no. [KM672662](#)), 25 genes with phage AM24 (97,137 bp, 146 ORFs; GenBank accession no. [KY000079](#)), and fewer than 18 genes with all other phages.

Analysis of phage B9 structural proteins. To determine the protein composition of the phage B9 particle, the structural components were precipitated, separated by electrophoresis, and trypsinized and the resulting peptides were analyzed by electrospray ionization-tandem mass spectrometry (Fig. 3). Mass spectrometry allowed the identification of 29 proteins, of which 27 had a coverage of over 5% and more than one unique peptide. Among these proteins, 13 had predicted function (e.g., tail fiber and minor and major capsid proteins), 8 had unknown function but were located in the morphogenetic phage module (Fig. 2C), and 6 were unique proteins without homologs (gp31, gp37, gp44, gp49, gp59, and gp60), generally closely located at the predicted morphogenetic phage module. The protein carrying the depolymerase domain (gp69) used in this study was also identified, suggesting that it is also part of the phage virion structure.

Identification of B9gp69 as a capsular depolymerase. The fact that phage B9 plaques are surrounded by halos on K45 strain lawns is indicative of bacterial cell decapsulation by depolymerases. We detected a pectate_lyase_3 domain (PF12708) in the C terminus of B9gp69 (Fig. 4A), although with low homology (E value, $4.9E-7$). We further proved that this is a structural protein that has no attributed function and shares relatively low identity only to *Acinetobacter* sp. proteins (<55% amino acid identity). To assess the activity of this protein, the C-terminal domain of B9gp69 was cloned, heterologously expressed, and tested using the spot-on-lawn method against *Acinetobacter* strains. Like phage B9, the recombinant depolymerase (B9gp69) is active against the K30 and K45 strains (Table 1). In the spot test, the enzyme was active down to a concentration of $0.01 \mu\text{M}$ on both capsular types (Fig. 4B).

Depolymerase functional analysis. The B9gp69 activity was also tested toward extracted exopolysaccharides (EPS) from the K30 and K45 sensitive strains and one K3 nonsensitive strain. In agreement with the above-described spot-on-lawn results, the enzyme was able to degrade polysaccharides only from the K30 and K45 strains and not

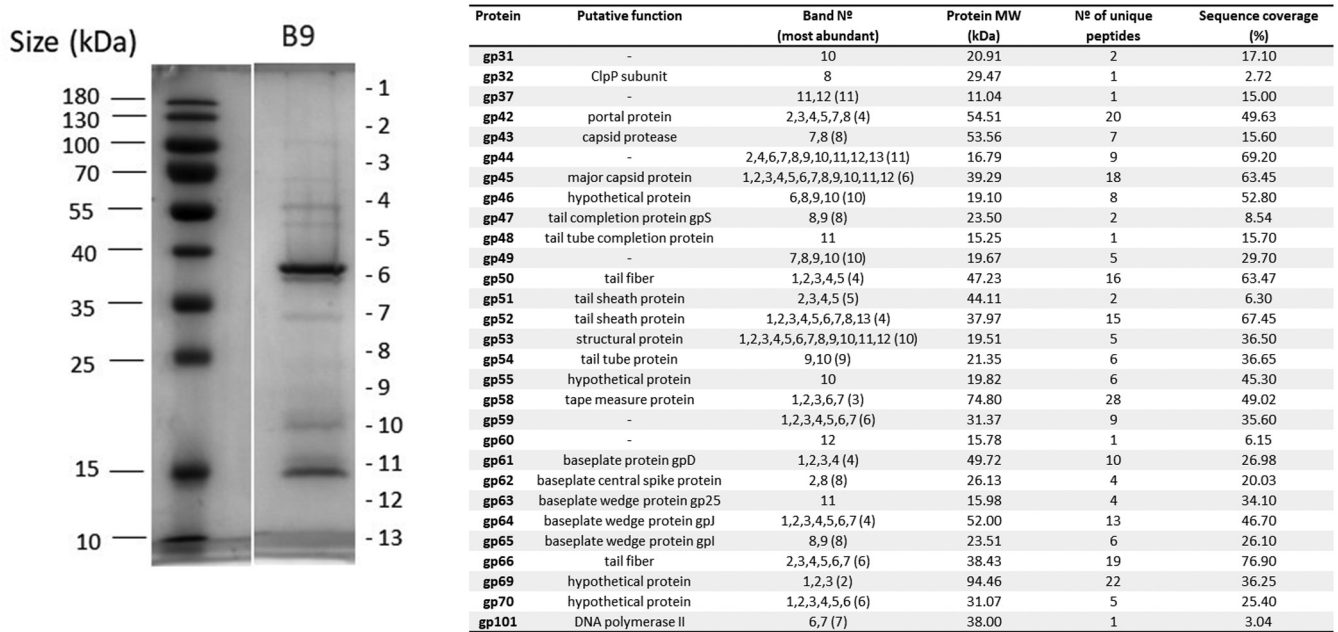


FIG 3 Analysis of phage B9 virion proteins. Structural proteins were separated on a 12% SDS-PAGE separation gel, alongside with a PageRuler prestained protein ladder. The entire lane was cut into 13 slices and trypsinized, and the resulting peptides were analyzed using liquid chromatography-electrospray ionization-tandem mass spectrometry. The resolved proteins are listed.

from the K3 strain (Fig. 5). Using EPS from the K45 strain, the enzyme activity was further characterized under different environmental conditions (pH, ionic strength, and temperature) (Fig. 6). The enzyme remained active in all pH values tested (pH 5 to 9), with an optimum around pH 5 to 7 (Fig. 6A). Interestingly, the enzyme was not affected by the presence of salt up to 500 mM (Fig. 6B). The enzyme was also shown to be mesophilic, exhibiting optimal activity between temperatures of 20°C and 60°C (Fig. 6C). At 70°C and 80°C, the enzyme displayed a slight or substantial reduction to 73% and 53% of activity.

To gain further insight into the structure of the depolymerase, we resorted to circular dichroism (CD) spectroscopy to assess the secondary structure content. The CD spectrum demonstrated two negative dichroic minimums, one between 218 and 220 nm and another less pronounced at 212 nm, with a positive dichroic maximum at 193 nm, which are signature peaks of an α -sheet content (Fig. 7A). In agreement, deconvolution analysis of the CD spectra using DichroWeb server demonstrated that

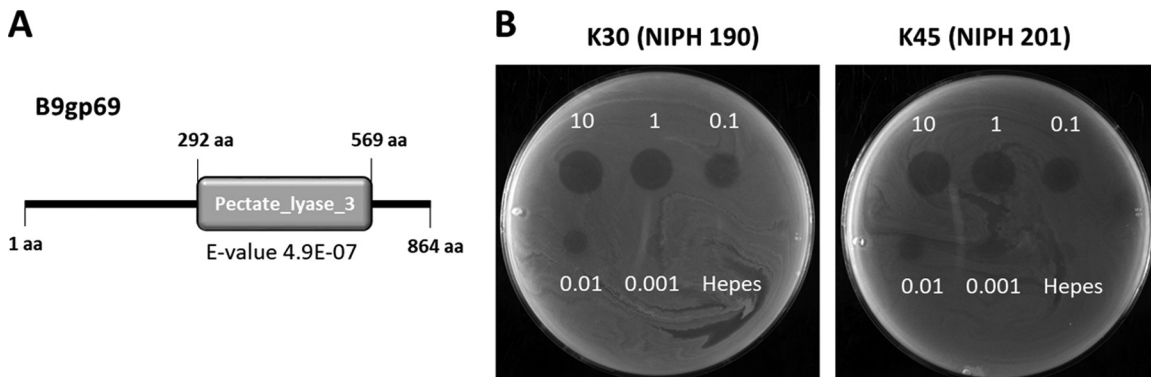


FIG 4 *In silico* and *in vitro* analysis of the depolymerase of phage B9. (A) Bioinformatics analysis using BLASTP and HHpred output. The depolymerase domain identified and cloned in this study corresponds to the phage genetic region from bp 775 to 2592 of ORF69. (B) Spot test of different micromolar concentrations of the B9gp69 on *Acinetobacter baumannii* K45 strain NIPH 210.

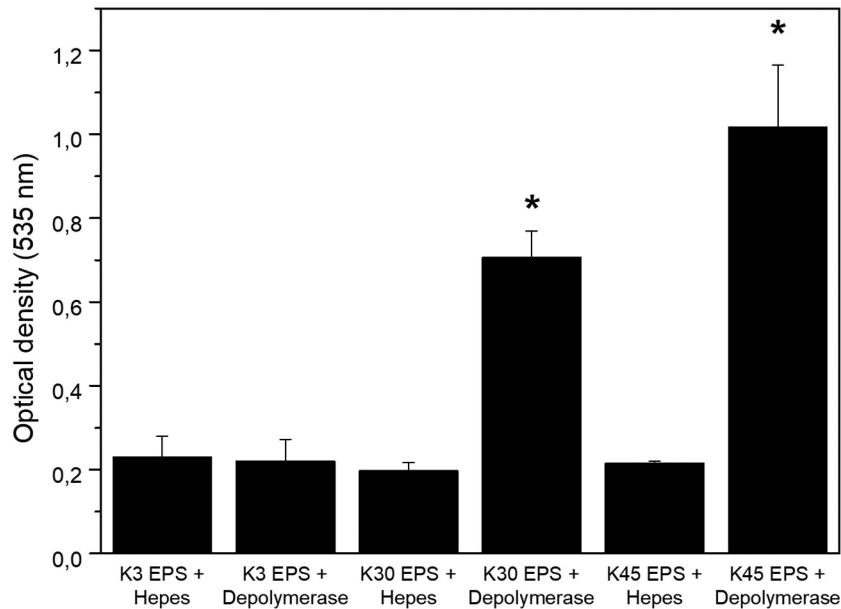


FIG 5 Depolymerase activity toward extracted exopolysaccharides (EPS). Purified EPS from depolymerase-sensitive strains K45 NIPH 201 and K30 NIPH 190 and nonsensitive strain K3 NIPH 501 were incubated with HEPES (untreated) or B9gp69 (treated) for 1 h at 37°C. EPS cleavage was quantified by the amount of sugar ends present using the DNS method. Significance was determined by a Student *t* test for comparison between the treated and the untreated groups. *, statistically different ($P < 0.01$).

B9gp69 folds 100% as α -helices. The CD was also employed to measure the secondary structure stability by monitoring transitions as a function of temperature, which indicated that B9gp69 unfolds at 51°C (Fig. 7B).

Role of depolymerase in phage adsorption. To clarify the role of the depolymerase in phage B9 infection, we performed adsorption experiments with phage B9 and hosts of different capsular types, with and without pretreatments with B9gp69 and in presence or absence of free EPS (Fig. 8). The phage adsorbed more than 93.8% to nontreated K45 cells, whereas it adsorbed only 25.3% to depolymerase-treated K45 cells ($P < 0.01$). Similarly, phage adsorbed 85.5% to K30 cells versus 17.8% to depolymerase-treated K30 cells. In both cases, additions of free EPS did not interfere with phage adsorption. For nonhost K3 (insensitive to both phage and enzyme), no phage adsorption to either wild-type or pretreated strain was observed.

Depolymerase cytotoxicity on human epithelium. To assess the safety of B9gp69, the cytotoxicity of the depolymerase toward human epithelial cells was tested. The epithelial cell line A549 was used, as the human respiratory tract is one of the main

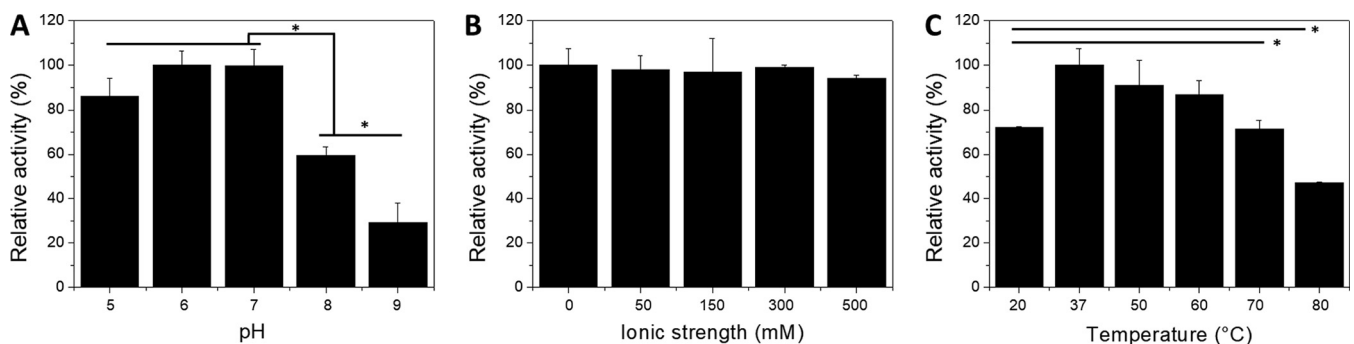


FIG 6 Depolymerase activity under different environmental conditions. The enzyme was incubated with EPS extracted from *Acinetobacter* strains at different pH values (5 to 9; 0 mM NaCl and 37°C) (A), ionic strengths (0 to 500 mM NaCl; pH 6 and 37°C) (B), and temperatures (37 to 80°C; pH 6 and 0 mM NaCl) (C). The results are expressed as relative activity, comparing with the best activity value obtained, pH 6, 0 mM, 37°C. *, statistically significant ($P < 0.05$).

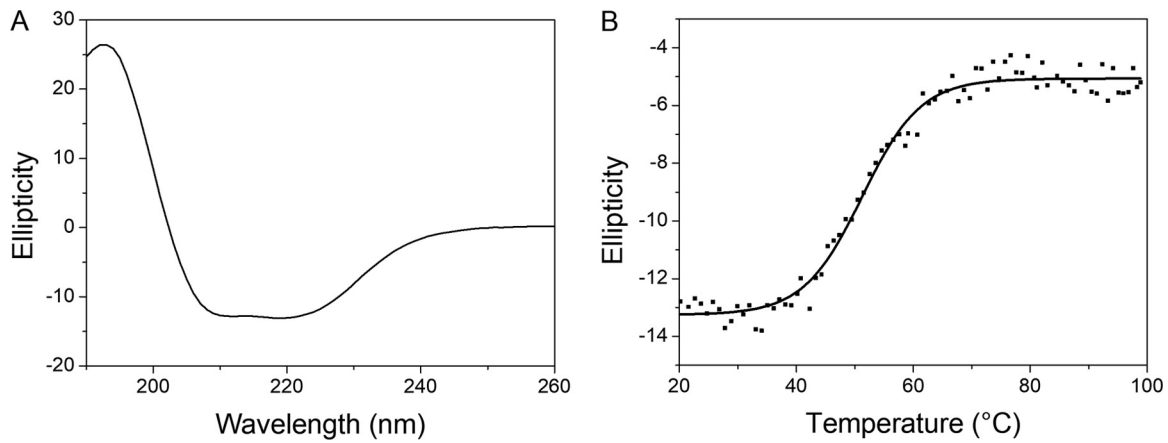


FIG 7 Circular dichroism analysis of the depolymerase. (A) CD spectrum measured in the far-UV (190 to 260 nm); (B) melting curve acquired at 218 nm with the protein (4 μ M) dialyzed in potassium phosphate buffer at pH 7.

targets of this pathogen (23). B9gp69 demonstrated a nontoxic effect toward the cells, as similar quantities of soluble formazan were detected in A549 cells after 24 h of exposure to the depolymerase (Fig. 9) as in cells under control conditions. Additionally, the numbers of treated and untreated bacterial cells colonizing A549 cells were similar, demonstrating a lack of antibacterial effect of B9gp69 (data not shown).

Serum sensitivity of depolymerase-treated bacteria. The capacity of the depolymerase to enhance bacterial susceptibility to serum killing was tested on the K45 strain (Fig. 10). When intact cells were added to serum, the bacterial load increased 2-fold. In contrast, B9gp69-pretreated cells incubated with serum were reduced below the detection limit (<10 CFU/ml). As expected, B9gp69 could not complement the serum killing activity against the K3 strain. This is a clear indication of the enhancing effect of B9gp69 on the bacterial susceptibility to human serum killing.

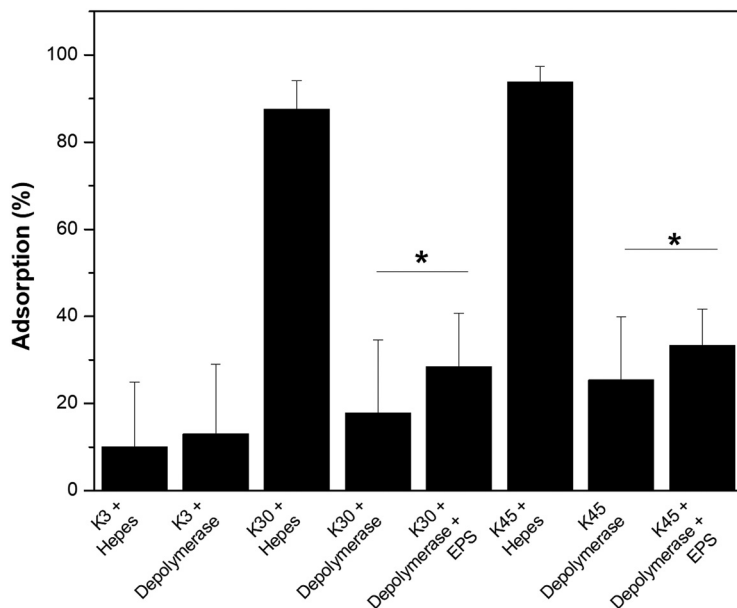


FIG 8 Phage adsorption. Phage B9 was adsorbed in K3, K30, and K40 using (i) wild-type cells, (ii) depolymerase-treated cells, and (iii) depolymerase-treated cells in the presence of free EPS (5 mg/ml). Results are expressed as residual PFU percentages in comparison with adsorption assays with untreated cells, as indicated on the x axis. Error bars represent SDs from three repeated experiments. Significance was determined by a Student *t* test for comparison between the treated and the untreated groups. *, statistically significant ($P < 0.01$).

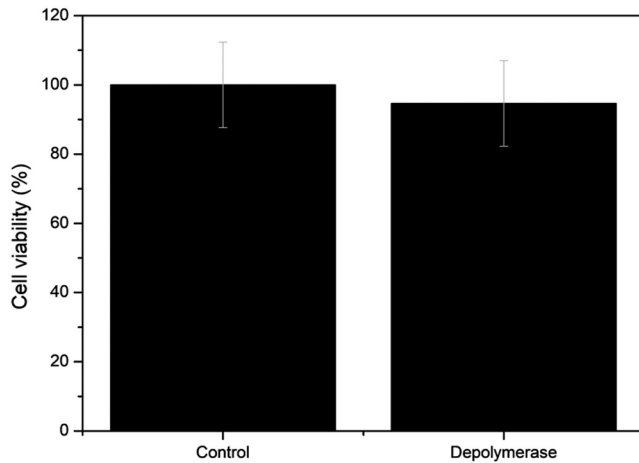


FIG 9 Cytotoxicity effect of the depolymerase on human epithelium. The cytotoxicity effect of the enzyme was measured by assessing the viability of human lung carcinoma cell line A549 (ATCC CCL-185) when incubated with B9gp69 for 24 h, measuring the soluble formazan produced by cellular reduction by MTS at 490 nm, after addition of the CellTiter 96 Aqueous One solution reagent. The results are expressed as percentage by comparing with HEPES as a control (=100% cell viability). *, statistically significant ($P < 0.05$).

Frequency of phage- and depolymerase-insensitive mutants. As the emergence of resistance is a key factor when considering phage therapy, the K45 strain was challenged with phage or B9gp69 for 24 h and evaluated for the appearance of insensitive phenotypes (Table 2). While the phage- and enzyme-free cultures displayed a steep growth curve, cultures infected with the phage demonstrated an initial decrease of cell density followed by regrowth after 8 to 9 h, a consequence of the development of phage-insensitive variants. For the culture incubated with the B9gp69, no antibacterial effect was observed.

Ten bacterial colonies of each culture were selected to assess sensitivity toward the phage or B9gp69. As expected, all 10 colonies grown free of phage and enzyme remained sensitive to both. For phage-challenged cultures, three colonies were insensitive to both phage and enzyme, and seven remained sensitive to both. Of these, three had a diminished efficiency of plating (EOP), while B9gp69 remained active at the

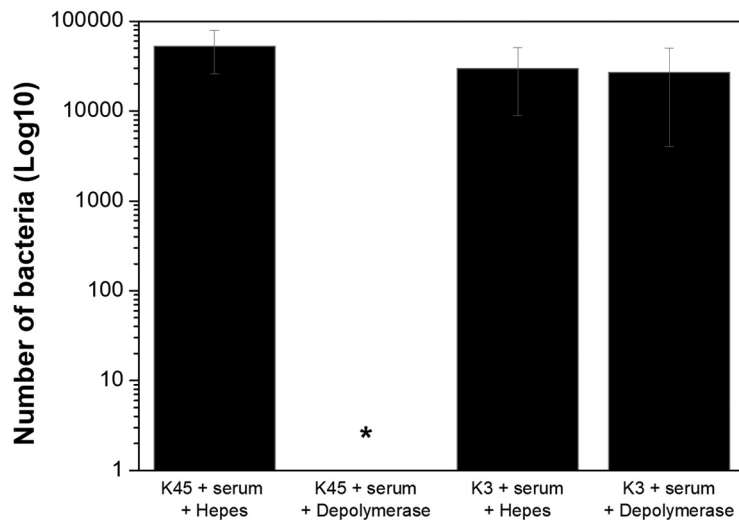


FIG 10 Effect of the depolymerase of phage B9 on bacterial susceptibility to serum killing. Host K45 and nonhost K3 susceptibility to killing by human serum was evaluated by adding only bacteria or bacteria pretreated with B9gp69. The enzyme was used at 0.1 μ M. Significance was determined by Student *t* test. *, $P < 0.001$.

TABLE 2 Activity spectrum of depolymerase B9gp69 on *A. baumannii* isolated in this study^a

Isolate no.	Incubation with SM buffer		Incubation with phage		Incubation with depolymerase	
	Phage (EOP)	Depolymerase	Phage (EOP)	Depolymerase	Phage (EOP)	Depolymerase
1	+ (high)	+	+ (high)	+	+ (high)	+
2	+ (high)	+	+ (high)	+	+ (high)	+
3	+ (high)	+	–	–	+ (high)	+
4	+ (high)	+	–	–	+ (high)	+
5	+ (high)	+	+ (low)	+	+ (high)	+
6	+ (high)	+	+ (high)	+	+ (high)	+
7	+ (high)	+	+ (low)	+	+ (high)	+
8	+ (high)	+	+ (low)	+	+ (high)	+
9	+ (high)	+	+ (high)	+	+ (high)	+
10	+ (high)	+	–	–	+ (high)	+

^aK45 NIPH 201 cells were incubated with SM buffer, phage, or B9gp69 and afterwards tested for their sensitivity against the phage or B9gp69 using drop tests. For the phage, the relative efficiency of plating (EOP) was calculated as the titer of the phage (PFU per milliliter) for each isolate divided by the titer for the propagating host and recorded as high (≥ 0.5) or low (< 0.5). EOP was also performed to distinguish productive infection (lysis) from lysis from without by the appearance of cell lysis only in the first dilution(s) for the latter case.

lowest concentration, 0.01 μ M. For B9gp69-challenged cultures, all 10 colonies remained sensitive to both phage and enzyme, indicating a lack of resistance development. Of note, the enzyme was found to be active after overnight incubation with K45 cells using drop tests (data not shown).

DISCUSSION

A. baumannii has become one of the priority human pathogens for the development of new antimicrobials due to its prevalence in hospital care units and increased multidrug resistance. Capsular polysaccharide represents an important virulence factor for most clinical isolates of Gram-negative and Gram-positive species (24) and presumably also for *A. baumannii* (11). To date, of 106 capsular types found in *A. baumannii*, only K1 from the *A. baumannii* strain AB307-0294 was recently shown to be a virulence factor (11). Furthermore, the prevalence of the 106 capsular types in clinical settings remains unknown due to the absence of implemented typing schemes (9). Studies on phage-encoded depolymerases and their use for recognition and removal of specific capsules of *A. baumannii* are necessary to develop novel typing and treatment schemes, as has been done for pathogens like *Klebsiella*, *Escherichia coli*, and *Pseudomonas* (15, 25–28). Here we demonstrate that the K45 capsular type is an important virulence factor and a protective barrier against the human immune system. We also demonstrate for the first time that capsular depolymerases have antivirulence properties against *A. baumannii*.

We isolated B9 myovirus from sewage samples, and this virus was able to infect only K45 strains and cause lysis from without on the K30 strain. We hypothesized the narrow host range to be a consequence of the phage using depolymerases to recognize specific host capsule, as recently demonstrated for several *A. baumannii* podoviruses (17, 18). Aiming to characterize this capsular depolymerase, we sequenced the genome of phage B9. Based on bioinformatics analysis, we demonstrated that phage B9 is a novel *A. baumannii*-infecting phage. It lacks relatedness at the genomic level ($< 1\%$) and shares limited gene content (< 31 out of 167 genes) only with *A. baumannii* myoviruses YMC13/03/R2096 and AM24, which were recently proposed to form a new genus named “R2096virus” (both share 117 genes) (29). Additionally, novel virion structural proteins were identified by mass spectrometry. Therefore, phage B9 is eligible to create a new genus within the subfamily *Tevenvirinae*.

Through screening of phage-encoding proteins and mass spectrometry, we found that B9gp69 is a structural protein with a conserved C-terminal pectate_lyase_3 domain of weak homology, a domain that has been previously shown to be responsible for decapsulation of bacterial cells (18). According to comparison with other *Acinetobacter* phages, this protein is likely a new tail spike (18). The recombinant depolymerase (B9gp69) harboring the pectate_lyase_3 domain was active on K30 and K45 strains. The K loci of the tested strains are flanked by *fkpA* and *lldP* genes, several conserved genes

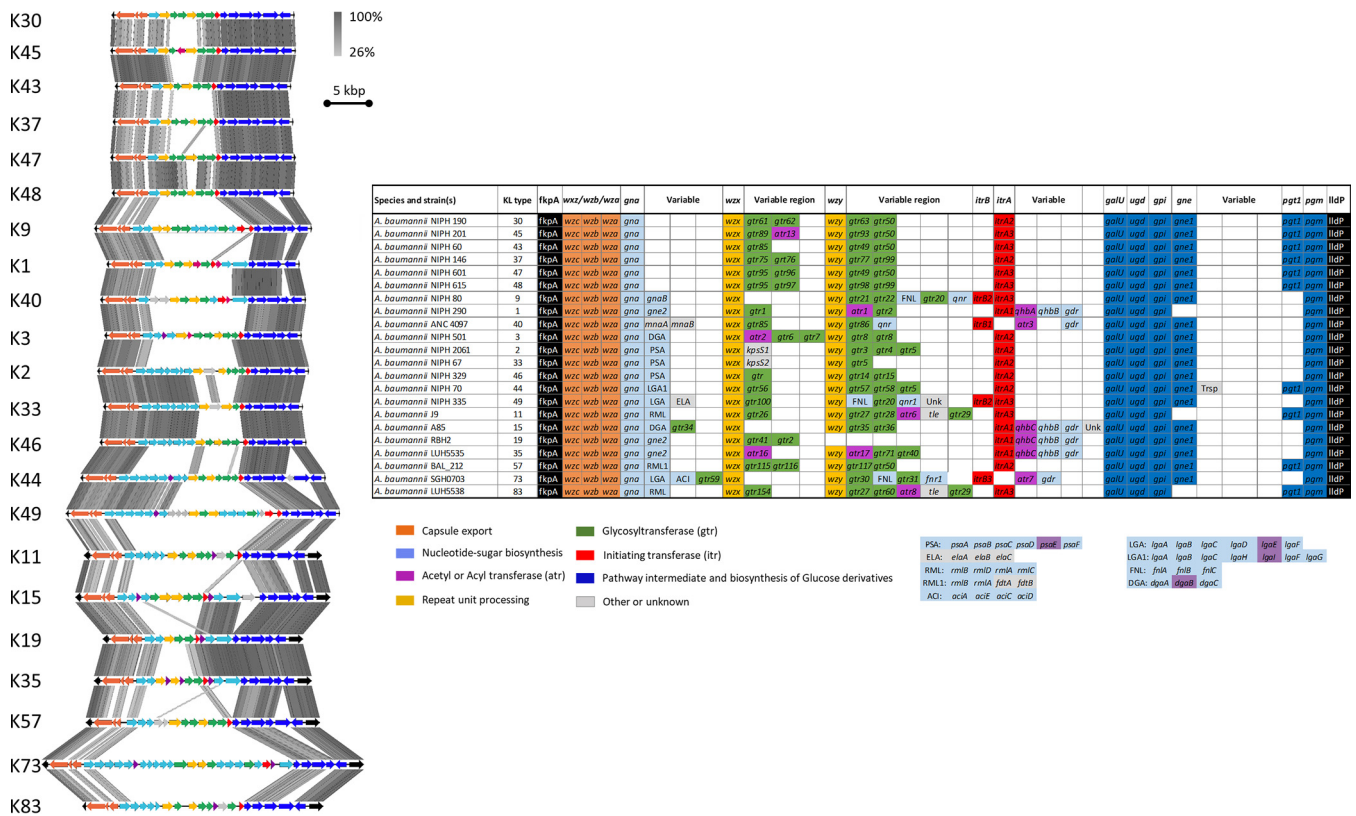


FIG 11 K locus variation of *Acinetobacter baumannii* strains. The capsular synthesis loci were represented with EasyFig drawn at scale (left) or using a table (right). Capsular polysaccharide clusters were annotated following the Hall-Kenyon nomenclature (22, 66, 67). The K locus genes are colored according to function. The K locus is flanked by *fkpA* and *lldP* genes marked in black. Loci are accessible by the GenBank entries listed in Table 3. Unk, gene with unknown function; Trsp, transposase.

involved in the capsule export and repeat unit processing, and nonconserved genes responsible for nucleotide sugar and glycosyltransferase biosynthesis are present (Fig. 11). Specially, several include genes for uncommon sugars, such as pseudaminic acid (*psa*) and legionaminic acid (*lag*), which are absent in K30 and K35 locus. At the structure level, we noticed that glucose-1-6-*N*-acetyl-D-glucosamine and *N*-acetyl-D-glucosamine-1-4-*N*-acetylgalactosamine are bonds shared only by K30 and K45 and are therefore possible cutting sites of B9gp69 (22). Other depolymerases encoded by *Klebsiella pneumoniae*- and *E. coli*-infecting phages were also found to degrade specific capsule types matching the host range of their parental phages (25). Even in the few examples in which phages encode multiple depolymerases for multiple capsule types, the phage host range matched to the sum of sensitive capsule types of the individual encoded depolymerases (15, 30).

After testing B9gp69 under several conditions, we demonstrated that it is highly active at various pH (5 to 9), ionic strengths (0 to 500 mM), and temperatures (20 to 80°C). This impressive tolerance to extreme conditions is probably related to the structural nature of phage depolymerases, which have been designed during evolution to endure harsh external environments in order to maintain phage infectivity. Interestingly, although B9gp69 remained active up to 80°C, its secondary structure unfolded at a much lower temperature (51°C). It is possible that the active center of B9gp69 remains available at high temperatures to cleave the capsular polymers, being independent of its secondary structure. We also noticed that the secondary content of B9gp69 made of α -helices is different from the typical beta-sheet-rich structures observed so far on other *K. pneumoniae* and *E. coli* phage depolymerases, which melt at higher temperatures (>65°C) (25, 31). Another important difference is that we used only the C-terminal region of the tail fiber gene, which contains the depolymerase activity, while all mentioned studies used the whole tail fiber gene.

We have also assessed the role of B9gp69 in phage adsorption. Phages typically use tail spikes or tail fiber proteins to recognize various bacterial receptors, from cell wall components (e.g., lipopolysaccharide and outer membrane proteins) to pili, flagella, and capsules (30, 32, 33). It is also common for phages to have a primary reversible and a secondary irreversible receptors (34–36). For phage B9, our results indicate that the capsule surrounding the cells is essential for adsorption, since the phage could no longer efficiently bind to B9gp69-pretreated K45 cells. The fact that the addition of crude EPS did not compromise phage adsorption indicates a strong therapeutic potential of the phage in the presence of free carbohydrates. Also, because phage B9 infects K45 but only makes lysis from without in K30, it is possible that these two capsules act as a primary phage receptor, with a distinct secondary and more internal receptor. Similar findings were previously reported for *E. coli* K1 phage, which infected only the wild-type strain with an intact polysialic acid capsule and not the capsule-deprived cells (32). More recently, similar results were also reported for a phage-borne depolymerase infecting *K. pneumoniae* and *Acinetobacter pittii* species (18, 30). Therefore, depolymerases recognize bacterial capsules as receptor for phage adsorption and are essential to initiate infection.

To assess the cytotoxicity and antivirulence effect of capsular B9gp69, we tested the enzyme in mammalian cells and human serum models. In the mammalian cell assay, the enzyme was found to be nontoxic. In the human serum assay, we observed that the K45 strain was resistant to killing by serum complement and that it could proliferate. Treatment with B9gp69 had a strong effect on the K45 strain, making it fully susceptible to serum killing. The lipopolysaccharide of *Acinetobacter* strains has been previously linked to the bacterium's increased resistance to the host immune system (37). Here we show that specific capsule polymers have also an important role in the immune system evasion. These results agree with previous studies with *K. pneumoniae* in which several capsular types (e.g., K1, K5, K8, K30, K64, and K69) were shown to be resistant to serum killing (26, 30, 38).

Considering the antivirulence and antiserum resistance properties of B9gp69, this enzyme is a potential antimicrobial for the control of *A. baumannii* infections. One of the major concerns about the development of novel antimicrobial strategies, among which phage therapy is included, is the repetition of the mistakes made with antibiotics, which resulted in the fast emergence of resistance. So in this study, we addressed this issue with both phage B9 and B9gp69. Bacteria were able to develop resistance to phage B9 but not to B9gp69, probably because the enzyme does not kill the cells and instead only degrades the extracellular capsule. It is also possible that the relatively low concentration of enzyme we used (0.1 μ M), due to expression limitations, was not enough to induce resistance. Nonetheless, this study showed the *in vitro* and *ex vivo* efficacy of a phage-derived capsular depolymerase from a new phage infecting *A. baumannii* able to reduce the bacterial virulence and sensitize the bacterium to serum killing. Here we provided further evidence that support the therapeutic potential of phage-derived depolymerases against *A. baumannii*, a major threat for human health.

MATERIALS AND METHODS

Bacterial strains. A panel of 21 *A. baumannii* strains were used covering a range of 22 different bacterial capsule types (K1 to K3, K9, K11, K15, K30, K33, K35, K37, K40, K43 to K49, K57, K73, and K83) (Table 3). They mostly belong to the collections of Alexandr Nemeč (NIPH and ANC strains) and of the Institut Pasteur (CIP strains) (39–47). All strains were routinely grown at 37°C in Trypticase soy broth (TSB) or in Trypticase soy agar (TSA; 1.5% [wt/vol] agar).

Phage isolation. Phage vB_AbM_B9 was isolated from a raw sewage wastewater treatment plant (Braga, Portugal) using an enrichment procedure as previously described (18), using K45 strain NIPH 201. Purified phage plaques were propagated in solid media, collected with SM buffer, filtered, purified with polyethylene glycol 8000 (PEG 8000)-NaCl and titrated following standard procedures (48).

Transmission electron microscopy. Phage particles were centrifuged (20,000 \times g, 1 h, and 4°C), washed, and suspended in tap water. A drop of phage solution was added onto copper grids provided with carbon-coated Formvar films, stained with 2% (wt/vol) uranyl acetate (pH 4.0), and observed with a Jeol JEM 1400 transmission electron microscope (TEM).

Phage sequencing and annotation. Phage B9 genomic DNA was extracted by phenol-chloroform as previously described (48). A DNA library was constructed using the KAPA DNA library preparation kit for Illumina and sequenced (100 bp in paired-end mode) using Illumina HiSeq platform (StabVida). Reads

TABLE 3 *Acinetobacter baumannii* strains used in this study^a

Strain classification and designation	Specimen	Locality and/or year of isolation	ST	K type	GenBank accession no.	Reference
<i>Acinetobacter baumannii</i> (n = 28)						
NIPH 501T (=ATCC 19606 ^T)	Urine	Before 1949	52	3	KB849970.1 (bp 174731–119233)	39
NIPH 60 (=CIP 110424)	Sputum	Praha, Czech Republic, 1992	34	43	KB849508.1 (bp 140959–120981)	39
NIPH 67 (=CIP 110425)	Tracheal secretion	Praha, Czech Republic, 1992	35	33	KB849903.1 (bp 1301423–1278652)	39
NIPH 70 (=CIP 110426)	Tracheal secretion	Praha, Czech Republic, 1992	36	44	KB849923.1 (bp 574942–546765)	39
NIPH 80 (=CIP 110427)	i.v. cannula	Praha, Czech Republic, 1993	37	9	KB849944.1 (bp 156383–131489)	39
NIPH 146 (=CIP 110428)	Wound	Praha, Czech Republic, 1993	25	37	KB849308.1 (bp 572444–592959)	39
NIPH 190 (=CIP 110429)	Tracheal secretion	Praha, Czech Republic, 1993	9	30	KB849477.1 (bp 592918–572137)	39
NIPH 201 (=CIP 110430)	Nasal swab	Liberec, Czech Republic, 1992	38	45	KB849844.1 (bp 365379–344305)	39
NIPH 329 (=CIP 110432)	Tracheal secretion	Tábor, Czech Republic, 1994	11	46	KB849871.1 (bp 2591085–2567472)	39
NIPH 335 (=CIP 110433)	Sputum	Tábor, Czech Republic, 1994	10	49	KB849886.1 (bp 1318556–1286966)	39
NIPH 528 (=CIP 110436 = RUH 134)	Urine	Rotterdam, the Netherlands, 1982	2	9	KB849906.1 (bp 78004–102899)	39
NIPH 601 (=CIP 110437)	Urine	Praha, Czech Republic, 1993	40	47	KB849894.1 (bp 3226845–3205785)	39
NIPH 615 (=CIP 110438)	Tracheal secretion	Praha, Czech Republic, 1994	12	48	KB849301.1 (bp 114143–93442)	39
NIPH 1734 (=CIP 110466)	Sputum	Mladá Boleslav, Czech Republic, 2001	15	49	KB849325.1 (bp 2998512–2965610)	39
NIPH 2390 (=RUH 2180)	Sputum	Nijmegen, the Netherlands, 1987	27	NA	NA	39
NIPH 2778 (=LUH 8088)	Sputum	Leiden, the Netherlands, 2002	48	NA	NA	39
NIPH 2783 (=LUH 8326)	Wound	Leiden, the Netherlands, 2002	18	NA	NA	39
NIPH 290 (=CIP 110431)	Urine	Příbram, Czech Republic, 1994	1	1	KB849940.1 (bp 126651–104645)	40
NIPH 2061 (=CIP 110467)	i.v. cannula	Příbram, Czech Republic, 2003	2	2	KB849309.1 (bp 77375–101575)	40
ANC 4097 (=CIP 110499)	Tracheal aspirate	Ustí nad Labem, Czech Republic, 2011	1	40	KB849962.1 (bp 39134–62621)	40
ANC 4373	Wound swab	Praha, Czech Republic, 2012	NA	NA	NA	39
J9	NA	Sydney, Australia, 1999	49	11	KF002790	42
A85	sputum	Sydney, Australia, 2003	1	15	KC118540 (bp 8456–36738)	43
RBH2	Other	Brisbane, Australia, 1999	111	19	KU165787	44
LUH5535	NA	NA	NA	35	KC526896	45
BAL_212	NA	Vietnam	52	57	KY434631	46
SGH0703	NA	Singapore, 2007	2	73	MF362178	47
LUH5538	NA	Germany	NA	83	KC526898	9

^aFor all strains, the specimen, origin, sequence type (ST) according to the multilocus sequence analysis, capsular type (K), and GenBank accession number are given. Sequence types refer to the Pasteur scheme. Allocation of the capsular genes and respective coordinates are provided in the GenBank accession no. column. i.v., intravenous.

were demultiplexed and *de novo* assembled into a single contig with an average coverage above 100× using Geneious R9 and were manually inspected. MyRAST (49) and tRNAscan-SE (50) were used to determine the ORFs and tRNAs, respectively. Encoded proteins were queried against protein sequences in BLASTP and HHpred (51) and for homology search and structured prediction. TMHMM (52) and HMMTOP (53) servers were used to predict transmembrane domains and SignalP (54) to identify possible signal peptide cleavage sites. Comparative genomic and proteomic analyses were performed with BLASTN or OrthoVenn (55), respectively, and visualized using Easyfig (56).

Mass spectrometry. Virion proteins were isolated by chloroform-methanol extraction (1:1:0.75 [vol/vol/vol]) on a PEG-purified phage stock ($>10^{10}$ PFU/ml). The extracted protein pellet was resuspended in loading buffer (40% [vol/vol] glycerol, 4% [wt/vol] SDS, 200 mM Tris-HCl [pH 6.8], 8 mM EDTA, 0.4% [wt/vol] bromophenol blue) and heated for 5 min at 95°C. The protein extract was then loaded and separated on a 12% SDS-PAGE gel. After visualization by staining the gel with Gelcode blue safe protein stain (Thermo Scientific), gel fragments covering the entire lane of the gel were excised and subjected to trypsin digestion according to the method of Shevchenko et al. (57). The samples were subsequently analyzed using nano-liquid chromatography-electrospray ionization-tandem mass spectrometry (nanoLC-ESI-MS/MS), and peptides were identified using SEQUEST (version 1.4.0.288; Thermo Finnigan) and Mascot (version 2.5; Matrix Science), based on a database containing all predicted phage proteins from a six-frame translation of the genome.

Depolymerase cloning and expression. The C-terminal part of the ORF69 coding for a depolymerase domain (genetic region from bp 775 to 2592 of ORF69) was amplified using Kapa HiFi (Kapa Biosystems) and forward (GGATCCAACCTAACTTAATTGCAACAAT [with BamHI restriction site]) and reverse (CTCGAGTTATGTGATAGTAATAAGTTAGCAGTTG [with XhoI restriction site]) primers. The amplified gene was cloned in a pTSL vector previously constructed with a SlyD leader protein and tobacco etch virus (TEV) recognition site in between the SlyD protein and the polylinker (58). *Escherichia coli* BL21 cells harboring the recombinant plasmid expressed the protein with 1 μ M isopropyl- β -D-thiogalactopyranoside (IPTG) at 37°C overnight. Cells were pelleted and suspended in lysis buffer (50 mM Tris-HCl [pH 8.0], 300 mM NaCl) and disrupted by three freeze-thaw cycles and sonication (8 to 10 cycles with 30-s pulses and 30-s pauses). The protein was purified by immobilized-metal affinity chromatography (Thermo Scientific) and incubated with a TEV protease overnight at 4°C in a protease/protein ratio of 1/100 (vol/vol) to cleave the SlyD leader protein. The protein was repurified using nickel magnetic beads for His 6 tag protein purification (Bimake) and dialyzed in 10 mM HEPES.

Phage and depolymerase activity spectrum. The spot-on-lawn method was used to screen the host range of activity of phage B9 and its recombinant depolymerase (B9gp69) toward a panel of *A. baumannii* strains of different capsular types (Table 3). Mid-log-phase bacteria were poured in TSA soft agar overlay plates (TSB with 0.6% [wt/vol] agar) to form lawns. After drying, 5 μ l of phage (10^8 PFU/ml) or of purified enzyme (1 μ M) was spotted onto the petri dishes and incubated at 37°C overnight. The visualization of clear spots or opaque zones (halos) on the bacterial lawn determined the presence of antibacterial activity for phage and B9gp69, respectively. For the phage, the relative efficiency of plating (EOP) was calculated by dividing the titer of the phage (PFU per milliliter) obtained in each isolate by the titer determined in the propagating host. EOP was recorded as high (≥ 0.5) or low (< 0.5).

Phage one-step-growth curve. One-step growth curve experiments were performed on K45 strain NIPH 201 exactly as previously described (59). Briefly, mid-exponential-phase cells were adjusted to an optical density at 620 nm (OD_{620}) of 1.0 and infected with phage using a multiplicity of infection (MOI) of 0.001. Phage was allowed to adsorb for 5 min at 37°C and 120 rpm (ES-20/60). The mixture was then pelleted (7,000 $\times g$, 5 min, and 4°C) and suspended in fresh TSB. Samples were repeatedly taken every 5 or 10 min for a total period of 1 h of infection to determine PFU.

Depolymerase degradation of extracted exopolysaccharides. Exopolysaccharides (EPS) were extracted from K30 strain NIPH 190, K45 strain NIPH 201, and K3 strain NIPH 501, using an adapted protocol (60). Briefly, *A. baumannii* strains were grown on 20 TSA plates supplemented with 0.5% glucose at 37°C for 5 days. Cells were then harvested by scraping with 2.5 ml of 0.9% (wt/vol) NaCl per plate. The suspension was incubated with 5% phenol and agitated with a stir bar for 6 h. Afterwards, cells were pelleted (10,000 $\times g$ for 10 min) and the supernatant containing the EPS was precipitated with 5 volumes of 95% ethanol overnight at -20°C . The precipitate was spun (6,000 $\times g$ for 10 min), suspended in distilled deionized water, and treated with DNase I (20 $\mu\text{g/ml}$) and RNase (40 $\mu\text{g/ml}$) at 37°C for 1 h. The digestion was quenched by heating at 65°C for 10 min, and samples were lyophilized.

The activity of the B9gp69 on extracted EPS was determined using the 3,5-dinitrosalicylic acid (DNS) test to quantify sugar reducing ends. EPS were dissolved into 20 mM concentrations of different buffer systems (sodium citrate [pH 5 to 6], HEPES [pH 7 to 8], and boric acid [pH 9]) to a final concentration of 5 mg/ml and incubated with the B9gp69 at 0.1 μM or with buffer (control) at 37°C for 1 h. At optimal pH, B9gp69 activity was also screened in different ionic strengths (0 to 500 mM NaCl concentration) and temperatures (20°C to 80°C) for 1 h. The reaction was stopped by heat inactivation (100°C for 15 min), and centrifugation was carried out (8,000 $\times g$ for 2 min) to remove the denatured enzyme. Afterwards, 100 μl of the DNS reagent at 10 mg/ml (Sigma-Aldrich) was added to an equal volume of the digested products and heated to 100°C for 5 min, and the absorbance was measured at 535 nm. Results were expressed as percent relative activity.

Circular dichroism spectroscopy. The secondary structure and the thermostability of the B9gp69 were analyzed by circular dichroism in the far-UV region, using a Jasco J-1500 CD spectrometer equipped with a water-cooled Peltier unit. The spectrum was obtained using proteins dialyzed in 10 mM potassium phosphate buffer (pH 7) to a concentration of 10 μM , from 190 to 250 nm, with 1-nm steps, a scanning speed of 20 nm/min, high sensitivity, and a 16-s response time. Three consecutive scans were recorded

from each sample and potassium phosphate buffer was used as blank for baseline correction. The secondary structures were estimated from spectra using the CDSSTR (61) and CONTINLL (62) routine of the DICHROWEB (63, 64) server run on the Set 4 set for a wavelength of 190 to 240 nm.

Thermal denaturation data were obtained by incrementation at 1°C/min and monitoring the change in ellipticity of the protein secondary structure at 215 nm, 218 nm, or 222 nm from 25°C to 90°C. The melting curves were plotted as a function of temperature and fitted to the Boltzmann sigmoidal function.

Phage adsorption onto depolymerase-treated cells. Mid-exponential-phase (OD_{620} of 0.4) growing cells of K30 strain NIPH 190, K45 strain NIPH 201, and K3 strain NIPH 501 were incubated with an equal volume of B9gp69 (0.1 μ M final concentration) or HEPES (for negative control) for 2 h at room temperature (RT). After, cells were spun ($8,000 \times g$ for 2 min) and washed twice with TSB. Phage was added at a multiplicity of infection of 0.001 with and without the presence of extracted EPS (5 mg/ml) and incubated at 37°C and 120 rpm for 5 min to allow adsorption to the cell surface. Samples were taken before and after centrifugation of the sample to determine total phage titer and the titer of nonadsorbed phage, respectively. Phage adsorption was calculated by subtracting the amount of nonadsorbed phage from the total amount of phage. The effect of B9gp69 on the phage capacity to adsorb to cells was analyzed and expressed as percent. Significance was determined by a Student *t* test for comparison between the treated and untreated groups.

Cytotoxicity assays. For toxicity and cell viability assays, the human lung carcinoma cell line A549 (ATCC CCL-185) was used. Cells were maintained in Dulbecco's modified Eagle's medium (DMEM; Biochrom) supplemented with 10% fetal bovine serum (FBS; Biochrom) and $1 \times$ ZellShield (Biochrom) at 37°C in a humidified atmosphere at 5% CO_2 (HERAccl 150). A549 cells were subcultured every 2 days at 80% confluence in T-flasks (Starstedt). For the assays, cells were seeded into 96-well microtiter plates at 5×10^5 cells/ml and incubated at 37°C and 5% CO_2 for 24 h. Cells were washed once with 10 mM phosphate-buffered saline (PBS) and exposed to (i) HEPES or (ii) B9gp69 (final concentration of 0.1 μ M). After incubation for 24 h, the cell culture medium was removed and the cells were washed once with 10 mM HEPES and then detached with trypsin-EDTA (Biochrom). The bacterial concentration was determined by CFU quantification, and mammalian cells were stained with trypan blue and counted using a Neubauer chamber (Marienfeld, Germany) and a microscope (Leica ATC 2000). The toxicity of B9gp69 was assessed by (i) determining the concentration of viable mammalian cells and (ii) quantifying the amount of soluble formazan produced by cellular reduction of 3-(4,5-dimethylthiazol-2-yl)-5-(3-carboxymethoxyphenyl)-2-(4-sulfophenyl)-2H-tetrazolium (MTS) for 1.5 h measured at 490 nm, after cell contact with the depolymerase and comparing it to that obtained for the negative control.

Human serum assay. The ability of the depolymerase to enhance bacterial susceptibility to serum killing was tested as previously described (65). Host K45 strain NIPH 201 and nonhost K3 strain NIPH 501 were grown to mid-exponential phase, diluted in TSB to 10^4 CFU/ml, and treated with HEPES, B9gp69, or heat-inactivated (100°C for 30 min) B9gp69 for 1 h at 37°C. Afterwards, human serum from healthy volunteers was added at a volume ratio of 1:3 and the culture was incubated for 1 h at 37°C. Survival of bacterial cells was determined by CFU counts.

Resistance development assay. The frequency of bacterial variants emerging with resistance to phage or B9gp69 was determined by incubating phage (MOI of 10) or B9gp69 (0.1 μ M end concentration) with $\sim 10^6$ CFU/ml of K45 strain NIPH 201 in TSB for 16 h (37°C, 120 rpm, ES-20/60). The cultures were plated to obtain isolated bacterial colonies. These were subcultured three times in TSA plates to guarantee that the colonies were free of phage and B9gp69. Then 10 colonies were picked to test the sensitivity toward both phage and B9gp69 using the spot-on-lawn method. Challenged bacteria were considered resistant when no inhibition halo was observed.

Accession number(s). The complete genome sequences of the *A. baumannii* phage vB_AbaM_B9 have been deposited in GenBank under accession number [MH133207](https://doi.org/10.1128/JVI.01163-18).

SUPPLEMENTAL MATERIAL

Supplemental material for this article may be found at <https://doi.org/10.1128/JVI.01163-18>.

SUPPLEMENTAL FILE 1, PDF file, 0.6 MB.

ACKNOWLEDGMENTS

This study was supported by the Portuguese Foundation for Science and Technology (FCT) under the scope of the strategic funding of UID/BIO/04469/2013 unit, COMPETE 2020 (POCI-01-0145-FEDER-006684) and the Projects PTDC/BBS-BSS/6471/2014 (POCI-01-0145-FEDER-016678) and PTDC/CVT-CVT/29628/2017 (POCI-01-0145-FEDER-029628). This work was also supported by the BioTecNorte operation (NORTE-01-0145-FEDER-000004) funded by the European Regional Development Fund under the scope of Norte2020—Programa Operacional Regional do Norte. H.O. and A.R.C. acknowledge FCT for grants SFRH/BPD/111653/2015 and SFRH/BPD/94648/2013, respectively. Support from Hercules Foundation project R-3986 for J.-P.N. is also acknowledged. The work of R.L. and M.B. was supported by a GOA grant from KU Leuven. J.-P.N. acknowledges the support of Hercules Foundation project R-3986.

We acknowledge Alexandr Nemeč (National Institute of Public Health, Prague, Czech Republic) and Ruth Hall (School of Life and Environmental Sciences, University of Sydney, Sydney, Australia), who kindly provided the *A. baumannii* strains.

We declare that we have no competing financial interests.

REFERENCES

- Joly-Guillou ML. 2005. Clinical impact and pathogenicity of *Acinetobacter*. *Clin Microbiol Infect* 11:868–873. <https://doi.org/10.1111/j.1469-0691.2005.01227.x>.
- Bonnin RA, Cuzon G, Poirel L, Nordmann P. 2013. Multidrug-resistant *Acinetobacter baumannii* clone, France. *Emerg Infect Dis* 19:822–823. <https://doi.org/10.3201/eid1905.121618>.
- Qureshi ZA, Hittle LE, O'Hara JA, Rivera JI, Syed A, Shields RK, Pasculle AW, Ernst RK, Doi Y. 2015. Colistin-resistant *Acinetobacter baumannii*: beyond carbapenem resistance. *Clin Infect Dis* 60:1295–1303. <https://doi.org/10.1093/cid/civ048>.
- Spinosa MR, Progidica C, Tala A, Cogli L, Alifano P, Bucci C. 2007. The *Neisseria meningitidis* capsule is important for intracellular survival in human cells. *Infect Immun* 75:3594–3603. <https://doi.org/10.1128/IAI.01945-06>.
- Zaragoza O, Chrisman CJ, Castelli MV, Frases S, Cuenca-Estrella M, Rodríguez-Tudela JL, Casadevall A. 2008. Capsule enlargement in *Cryptococcus neoformans* confers resistance to oxidative stress suggesting a mechanism for intracellular survival. *Cell Microbiol* 10:2043–2057. <https://doi.org/10.1111/j.1462-5822.2008.01186.x>.
- Yoshida K, Matsumoto T, Tateda K, Uchida K, Tsujimoto S, Yamaguchi K. 2000. Role of bacterial capsule in local and systemic inflammatory responses of mice during pulmonary infection with *Klebsiella pneumoniae*. *J Med Microbiol* 49:1003–1010. <https://doi.org/10.1099/0022-1317-49-11-1003>.
- Llobet E, Tomas JM, Bengoechea JA. 2008. Capsule polysaccharide is a bacterial decoy for antimicrobial peptides. *Microbiology* 154:3877–3886. <https://doi.org/10.1099/mic.0.2008/022301-0>.
- Geisinger E, Isberg RR. 2015. Antibiotic modulation of capsular exopolysaccharide and virulence in *Acinetobacter baumannii*. *PLoS Pathog* 11:e1004691. <https://doi.org/10.1371/journal.ppat.1004691>.
- Kenyon JJ, Shashkov AS, Senchenkova SN, Shneider MM, Liu B, Popova AV, Arbatsky NP, Miroshnikov KA, Wang L, Knirel YA, Hall RM. 2017. *Acinetobacter baumannii* K11 and K83 capsular polysaccharides have the same 6-deoxy-L-talose-containing pentasaccharide K units but different linkages between the K units. *Int J Biol Macromol* 103:648–655. <https://doi.org/10.1016/j.ijbiomac.2017.05.082>.
- Lees-Miller RG, Iwashkiw JA, Scott NE, Seper A, Vinogradov E, Schild S, Feldman MF. 2013. A common pathway for O-linked protein-glycosylation and synthesis of capsule in *Acinetobacter baumannii*. *Mol Microbiol* 89:816–830. <https://doi.org/10.1111/mmi.12300>.
- Russo TA, Luke NR, Beanan JM, Olson R, Sauberman SL, MacDonald U, Schultz LW, Umland TC, Campagnari AA. 2010. The K1 capsular polysaccharide of *Acinetobacter baumannii* strain 307-0294 is a major virulence factor. *Infect Immun* 78:3993–4000. <https://doi.org/10.1128/IAI.00366-10>.
- Drulis-Kawa Z, Majkowska-Skrobek G, Maciejewska B. 2015. Bacteriophages and phage-derived proteins—application approaches. *Curr Med Chem* 22:1757–1773.
- Pires DP, Oliveira H, Melo LD, Sillankorva S, Azeredo J. 2016. Bacteriophage-encoded depolymerases: their diversity and biotechnological applications. *Appl Microbiol Biotechnol* 100:2141–2151. <https://doi.org/10.1007/s00253-015-7247-0>.
- Yan J, Mao J, Xie J. 2014. Bacteriophage polysaccharide depolymerases and biomedical applications. *BioDrugs* 28:265–274. <https://doi.org/10.1007/s40259-013-0081-y>.
- Pan YJ, Lin TL, Chen CC, Tsai YT, Cheng YH, Chen YY, Hsieh PF, Lin YT, Wang JT. 2017. *Klebsiella* phage ΦK64-1 encodes multiple depolymerases for multiple host capsular types. *J Virol* 91:e02457-16. <https://doi.org/10.1128/JVI.02457-16>.
- Lai MJ, Chang KC, Huang SW, Luo CH, Chiou PY, Wu CC, Lin NT. 2016. The tail associated protein of *Acinetobacter baumannii* phage PhiAB6 is the host specificity determinant possessing exopolysaccharide depolymerase activity. *PLoS One* 11:e0153361. <https://doi.org/10.1371/journal.pone.0153361>.
- Popova AV, Lavysch DG, Klimuk EI, Edelstein MV, Bogun AG, Shneider MM, Goncharov AE, Leonov SV, Severinov KV. 2017. Novel Fli-like viruses infecting *Acinetobacter baumannii*—vB_AbaP_AS11 and vB_AbaP_AS12—characterization, comparative genomic analysis, and host-recognition strategy. *Viruses* 9:188. <https://doi.org/10.3390/v9070188>.
- Oliveira H, Costa AR, Konstantinides N, Ferreira A, Akturk E, Sillankorva S, Nemeč A, Shneider M, Dotsch A, Azeredo J. 2017. Ability of phages to infect *Acinetobacter calcoaceticus*-*Acinetobacter baumannii* complex species through acquisition of different pectate lyase depolymerase domains. *Environ Microbiol* 19:5060–5077. <https://doi.org/10.1111/1462-2920.13970>.
- Merabishvili M, Vandenheuvel D, Kropinski AM, Mast J, De Vos D, Verbeken G, Noben JP, Lavigne R, Vaneechoutte M, Pirnay JP. 2014. Characterization of newly isolated lytic bacteriophages active against *Acinetobacter baumannii*. *PLoS One* 9:e104853. <https://doi.org/10.1371/journal.pone.0104853>.
- Peng F, Mi Z, Huang Y, Yuan X, Niu W, Wang Y, Hua Y, Fan H, Bai C, Tong Y. 2014. Characterization, sequencing and comparative genomic analysis of vB_AbaM-IME-AB2, a novel lytic bacteriophage that infects multidrug-resistant *Acinetobacter baumannii* clinical isolates. *BMC Microbiol* 14:181. <https://doi.org/10.1186/1471-2180-14-181>.
- Hernandez-Morales AC, Lessor LL, Wood TL, Migl D, Mijalis EM, Russell WK, Young RF, Gill JJ. 2018. Genomic and biochemical characterization of *Acinetobacter* podophage petty reveals a novel lysis mechanism and tail-associated depolymerase activity. *J Virol* 92:e01064-17. <https://doi.org/10.1128/JVI.01064-17>.
- Shashkov AS, Kenyon JJ, Arbatsky NP, Shneider MM, Popova AV, Miroshnikov KA, Volozhantsev NV, Knirel YA. 2015. Structures of three different neutral polysaccharides of *Acinetobacter baumannii*, NIPH190, NIPH201, and NIPH615, assigned to K30, K45, and K48 capsule types, respectively, based on capsule biosynthesis gene clusters. *Carbohydr Res* 417:81–88. <https://doi.org/10.1016/j.carres.2015.09.004>.
- Peleg AY, Seifert H, Paterson DL. 2008. *Acinetobacter baumannii*: emergence of a successful pathogen. *Clin Microbiol Rev* 21:538–582. <https://doi.org/10.1128/CMR.00058-07>.
- Taylor CM, Roberts IS. 2005. Capsular polysaccharides and their role in virulence. *Contrib Microbiol* 12:55–66. <https://doi.org/10.1159/000081689>.
- Majkowska-Skrobek G, Latka A, Berisio R, Maciejewska B, Squeglia F, Romano M, Lavigne R, Struve C, Drulis-Kawa Z. 2016. Capsule-targeting depolymerase, derived from *Klebsiella* KP36 phage, as a tool for the development of anti-virulent strategy. *Viruses* 8:324. <https://doi.org/10.3390/v8120324>.
- Pan YJ, Lin TL, Lin YT, Su PA, Chen CT, Hsieh PF, Hsu CR, Chen CC, Hsieh YC, Wang JT. 2015. Identification of capsular types in carbapenem-resistant *Klebsiella pneumoniae* strains by wzc sequencing and implications for capsule depolymerase treatment. *Antimicrob Agents Chemother* 59:1038–1047. <https://doi.org/10.1128/AAC.03560-14>.
- Olszak T, Shneider MM, Latka A, Maciejewska B, Browning C, Sycheva LV, Cornelissen A, Danis-Włodarczyk K, Senchenkova SN, Shashkov AS, Gula G, Arabski M, Wasik S, Miroshnikov KA, Lavigne R, Leiman PG, Knirel YA, Drulis-Kawa Z. 2017. The O-specific polysaccharide lyase from the phage LKA1 tailspike reduces *Pseudomonas* virulence. *Sci Rep* 7:16302. <https://doi.org/10.1038/s41598-017-16411-4>.
- Lin H, Paff ML, Molineux IJ, Bull JJ. 2017. Therapeutic application of phage capsule depolymerases against K1, K5, and K30 capsulated *E. coli* in mice. *Front Microbiol* 8:2257. <https://doi.org/10.3389/fmicb.2017.02257>.
- Turner D, Ackermann HW, Kropinski AM, Lavigne R, Sutton JM, Reynolds DM. 2017. Comparative analysis of 37 *Acinetobacter* bacteriophages. *Viruses* 10:5. <https://doi.org/10.3390/v10010005>.
- Hsieh PF, Lin HH, Lin TL, Chen YY, Wang JT. 2017. Two T7-like bacteriophages, K5-2 and K5-4, each encodes two capsule depolymerases: isolation and functional characterization. *Sci Rep* 7:4624. <https://doi.org/10.1038/s41598-017-04644-2>.
- Guo Z, Huang J, Yan G, Lei L, Wang S, Yu L, Zhou L, Gao A, Feng X, Han W, Gu J, Yang J. 2017. Identification and characterization of Dpo42, a

- novel depolymerase derived from the *Escherichia coli* phage vB_EcoM_ECOO78. *Front Microbiol* 8:1460.
32. Scholl D, Rogers S, Adhya S, Merrill CR. 2001. Bacteriophage K1-5 encodes two different tail fiber proteins, allowing it to infect and replicate on both K1 and K5 strains of *Escherichia coli*. *J Virol* 75:2509–2515. <https://doi.org/10.1128/JVI.75.6.2509-2515.2001>.
 33. Cornelissen A, Ceyssens PJ, Krylov VN, Noben JP, Volckaert G, Lavigne R. 2012. Identification of EPS-degrading activity within the tail spikes of the novel *Pseudomonas putida* phage AF. *Virology* 434:251–256. <https://doi.org/10.1016/j.virol.2012.09.030>.
 34. Marti R, Zurfluh K, Hagens S, Pianezzi J, Klumpp J, Loessner MJ. 2013. Long tail fibres of the novel broad-host-range T-even bacteriophage S16 specifically recognize *Salmonella* OmpC. *Mol Microbiol* 87:818–834. <https://doi.org/10.1111/mmi.12134>.
 35. Parent KN, Erb ML, Cardone G, Nguyen K, Gilcrease EB, Porcek NB, Pogliano J, Baker TS, Casjens SR. 2014. OmpA and OmpC are critical host factors for bacteriophage Sf6 entry in *Shigella*. *Mol Microbiol* 92:47–60. <https://doi.org/10.1111/mmi.12536>.
 36. Golomidova AK, Kulikov EE, Prokhorov NS, Guerrero-Ferreira RC, Knirel YA, Kostryukova ES, Tarasyan KK, Letarov AV. 2016. Branched lateral tail fiber organization in T5-like bacteriophages DT57C and DT571/2 is revealed by genetic and functional analysis. *Viruses* 8:26. <https://doi.org/10.3390/v8010026>.
 37. Panilaitis B, Johri A, Blank W, Kaplan D, Fuhrman J. 2002. Adjuvant activity of emulsan, a secreted lipopolysaccharide from *Acinetobacter calcoaceticus*. *Clin Diagn Lab Immunol* 9:1240–1247.
 38. Lin TL, Hsieh PF, Huang YT, Lee WC, Tsai YT, Su PA, Pan YJ, Hsu CR, Wu MC, Wang JT. 2014. Isolation of a bacteriophage and its depolymerase specific for K1 capsule of *Klebsiella pneumoniae*: implication in typing and treatment. *J Infect Dis* 210:1734–1744. <https://doi.org/10.1093/infdis/jiu332>.
 39. Nemeč A, Krizova L, Maixnerova M, van der Reijden TJ, Deschaght P, Passet V, Vanechoutte M, Brisse S, Dijkshoorn L. 2011. Genotypic and phenotypic characterization of the *Acinetobacter calcoaceticus*-*Acinetobacter baumannii* complex with the proposal of *Acinetobacter pittii* sp. nov. (formerly *Acinetobacter* genomic species 3) and *Acinetobacter nosocomialis* sp. nov. (formerly *Acinetobacter* genomic species 13TU). *Res Microbiol* 162:393–404. <https://doi.org/10.1016/j.resmic.2011.02.006>.
 40. Touchon M, Cury J, Yoon EJ, Krizova L, Cerqueira GC, Murphy C, Feldgarden M, Wortman J, Clermont D, Lambert T, Grillot-Courvalin C, Nemeč A, Courvalin P, Rocha EP. 2014. The genomic diversification of the whole *Acinetobacter* genus: origins, mechanisms, and consequences. *Genome Biol Evol* 6:2866–2882. <https://doi.org/10.1093/gbe/evu225>.
 41. Nemeč A, Krizova L, Maixnerova M, Sedo O, Brisse S, Higgins PG. 2015. *Acinetobacter seifertii* sp. nov., a member of the *Acinetobacter calcoaceticus*-*Acinetobacter baumannii* complex isolated from human clinical specimens. *Int J Syst Evol Microbiol* 65:934–942. <https://doi.org/10.1099/ijs.0.000043>.
 42. Hamidian M, Hall RM. 2014. Tn6168, a transposon carrying an ISAb1-activated ampC gene and conferring cephalosporin resistance in *Acinetobacter baumannii*. *J Antimicrob Chemother* 69:77–80. <https://doi.org/10.1093/jac/dkt312>.
 43. Hamidian M, Kenyon JJ, Holt KE, Pickard D, Hall RM. 2014. A conjugative plasmid carrying the carbapenem resistance gene blaOXA-23 in AbaR4 in an extensively resistant GC1 *Acinetobacter baumannii* isolate. *J Antimicrob Chemother* 69:2625–2628. <https://doi.org/10.1093/jac/dku188>.
 44. Kenyon JJ, Shneider MM, Senchenkova SN, Shashkov AS, Siniagina MN, Malanin SY, Popova AV, Miroshnikov KA, Hall RM, Knirel YA. 2016. K19 capsular polysaccharide of *Acinetobacter baumannii* is produced via a Wzy polymerase encoded in a small genomic island rather than the KL19 capsule gene cluster. *Microbiology* 162:1479–1489. <https://doi.org/10.1099/mic.0.000313>.
 45. Shashkov AS, Liu B, Kenyon JJ, Popova AV, Shneider MM, Senchenkova SN, Arbatsky NP, Miroshnikov KA, Wang L, Knirel YA. 2017. Structures of the K35 and K15 capsular polysaccharides of *Acinetobacter baumannii* LUH5535 and LUH5554 containing amino and diamino uronic acids. *Carbohydr Res* 448:28–34. <https://doi.org/10.1016/j.carres.2017.05.017>.
 46. Kenyon JJ, Kasimova AA, Shashkov AS, Hall RM, Knirel YA. 2018. *Acinetobacter baumannii* isolate BAL_212 from Vietnam produces the K57 capsular polysaccharide containing a rarely occurring amino sugar N-acetylviuosamine. *Microbiology* 164:217–220. <https://doi.org/10.1099/mic.0.000598>.
 47. Kenyon JJ, Notaro A, Hsu LY, De Castro C, Hall RM. 2017. 5,7-Di-N-acetyl-8-epiacinetaminic acid: a new non-2-ulosonic acid found in the K73 capsule produced by an *Acinetobacter baumannii* isolate from Singapore. *Sci Rep* 7:11357. <https://doi.org/10.1038/s41598-017-11166-4>.
 48. Sambrook J, Russell DW. 2001. *Molecular cloning: a laboratory manual*, 3rd ed. Cold Spring Harbor Laboratory Press, Cold Spring Harbor, NY.
 49. Aziz RK, Bartels D, Best AA, DeJongh M, Disz T, Edwards RA, Formsmma K, Gerdes S, Glass EM, Kubal M, Meyer F, Olsen GJ, Olson R, Osterman AL, Overbeek RA, McNeil LK, Paarmann D, Paczian T, Parrello B, Pusch GD, Reich C, Stevens R, Vassieva O, Vonstein V, Wilke A, Zagnitko O. 2008. The RAST server: rapid annotations using subsystems technology. *BMC Genomics* 9:75. <https://doi.org/10.1186/1471-2164-9-75>.
 50. Lowe TM, Eddy SR. 1997. tRNAscan-SE: a program for improved detection of transfer RNA genes in genomic sequence. *Nucleic Acids Res* 25:955–964.
 51. Soding J, Biegert A, Lupas AN. 2005. The HHpred interactive server for protein homology detection and structure prediction. *Nucleic Acids Res* 33:W244–W248. <https://doi.org/10.1093/nar/gki408>.
 52. Kall L, Sonnhammer EL. 2002. Reliability of transmembrane predictions in whole-genome data. *FEBS Lett* 532:415–418.
 53. Tusnady GE, Simon I. 2001. The HMMTOP transmembrane topology prediction server. *Bioinformatics* 17:849–850.
 54. Bendtsen JD, Nielsen H, von Heijne G, Brunak S. 2004. Improved prediction of signal peptides: SignalP 3.0. *J Mol Biol* 340:783–795. <https://doi.org/10.1016/j.jmb.2004.05.028>.
 55. Wang Y, Coleman-Derr D, Chen G, Gu YQ. 2015. OrthoVenn: a web server for genome wide comparison and annotation of orthologous clusters across multiple species. *Nucleic Acids Res* 43:W78–W84. <https://doi.org/10.1093/nar/gkv487>.
 56. Sullivan MJ, Petty NK, Beatson SA. 2011. Easyfig: a genome comparison visualizer. *Bioinformatics* 27:1009–1010. <https://doi.org/10.1093/bioinformatics/btr039>.
 57. Shevchenko A, Wilm M, Vorm O, Mann M. 1996. Mass spectrometric sequencing of proteins silver-stained polyacrylamide gels. *Anal Chem* 68:850–858.
 58. Taylor NMI, Prokhorov NS, Guerrero-Ferreira RC, Shneider MM, Browning C, Goldie KN, Stahlberg H, Leiman PG. 2016. Structure of the T4 base-plate and its function in triggering sheath contraction. *Nature* 533:346. <https://doi.org/10.1038/nature17971>.
 59. Oliveira H, Pinto G, Oliveira A, Oliveira C, Faustino MA, Briers Y, Domingues L, Azeredo J. 2016. Characterization and genome sequencing of a *Citrobacter freundii* phage Cfp1 harboring a lysin active against multidrug-resistant isolates. *Appl Microbiol Biotechnol* 100:10543–10553. <https://doi.org/10.1007/s00253-016-7858-0>.
 60. Lee IM, Tu IF, Yang FL, Ko TP, Liao JH, Lin NT, Wu CY, Ren CT, Wang AHJ, Chang CM, Huang KF, Wu SH. 2017. Structural basis for fragmenting the exopolysaccharide of *Acinetobacter baumannii* by bacteriophage Phi AB6 tailspike protein. *Sci Rep* 7:42711. <https://doi.org/10.1038/srep42711>.
 61. Compton LA, Johnson WC. 1986. Analysis of protein circular-dichroism spectra for secondary structure using a simple matrix multiplication. *Anal Biochem* 155:155–167.
 62. Vanstokkum IHM, Spoelder HJW, Bloemendal M, Vangrondele R, Groen FCA. 1990. Estimation of protein secondary structure and error analysis from circular-dichroism spectra. *Anal Biochem* 191:110–118. [https://doi.org/10.1016/0003-2697\(90\)90396-Q](https://doi.org/10.1016/0003-2697(90)90396-Q).
 63. Whitmore L, Wallace BA. 2004. DICHROWEB, an online server for protein secondary structure analyses from circular dichroism spectroscopic data. *Nucleic Acids Res* 32:W668–W673. <https://doi.org/10.1093/nar/gkh371>.
 64. Whitmore L, Wallace BA. 2008. Protein secondary structure analyses from circular dichroism spectroscopy: methods and reference databases. *Biopolymers* 89:392–400. <https://doi.org/10.1002/bip.20853>.
 65. Fang CT, Chuang YP, Shun CT, Chang SC, Wang JT. 2004. A novel virulence gene in *Klebsiella pneumoniae* strains causing primary liver abscess and septic metastatic complications. *J Exp Med* 199:697–705. <https://doi.org/10.1084/jem.20030857>.
 66. Kenyon JJ, Hall RM. 2013. Variation in the complex carbohydrate biosynthesis loci of *Acinetobacter baumannii* genomes. *PLoS One* 8:e62160. <https://doi.org/10.1371/journal.pone.0062160>.
 67. Arbatsky NP, Shneider MM, Kenyon JJ, Shashkov AS, Popova AV, Miroshnikov KA, Volozhantsev NV, Knirel YA. 2015. Structure of the neutral capsular polysaccharide of *Acinetobacter baumannii* NIPH146 that carries the KL37 capsule gene cluster. *Carbohydr Res* 413:12–15. <https://doi.org/10.1016/j.carres.2015.05.003>.